ACS APPLIED MATERIALS & INTERFACES

Research Article

www.acsami.org

Highly Efficient Electrochemical Responses on Single Crystalline Ruthenium–Vanadium Mixed Metal Oxide Nanowires

Sung Hee Chun,[†,∥] Hyun-A Choi,[†,∥] Minkyung Kang,[†] Moonjee Koh,[†] Nam-Suk Lee,[‡] Sang Cheol Lee,[§] Minyung Lee,[†] Youngmi Lee,[†] Chongmok Lee,*[,†] and Myung Hwa Kim*[,†]

[†]Department of Chemistry & Nano Science, Global Top5 Research Program, Ewha Womans University, Seoul 120-750, Korea

[‡]National Center for Nanomaterials Technology (NCNT), Pohang University of Science and Technology (POSTECH), Pohang 790-784, Korea

[§]Robotic Research Division, Daegu Gyeongbok Insititute of Science & Technology (DGIST), Dalseong 711-873, Korea

Supporting Information

ABSTRACT: Highly efficient single crystalline ruthenium–vanadium mixed metal oxide ($Ru_{1-x}V_xO_2$, $0 \le x \le 1$) nanowires were prepared on a SiO_2 substrate and a commercial Au microelectrode for the first time through a vapor-phase transport process by adjusting the mixing ratios of RuO_2 and VO_2 precursors. Single crystalline $Ru_{1-x}V_xO_2$ nanowires show homogeneous solid-solution characteristics as well as the distinct feature of having remarkably narrow dimensional distributions. The electrochemical observations of a $Ru_{1-x}V_xO_2$ (x = 0.28 and 0.66)-decorated Au microelectrode using cyclic voltammetry (CV) and electrochemical impedance spectroscopy (EIS) demonstrate favorable charge-transfer kinetics of $[Fe(CN)_6]^{3-/4-}$ and $Ru(NH_3)_6^{3+/2+}$ couples compared to that of a bare Au microelectrode. The catalytic activity of $Ru_{1-x}V_xO_2$ for oxygen and H_2O_2 reduction at neutral pH increases as the fraction of vanadium increases within our experimental conditions, which might be useful in the area of biofuel cells and biosensors.

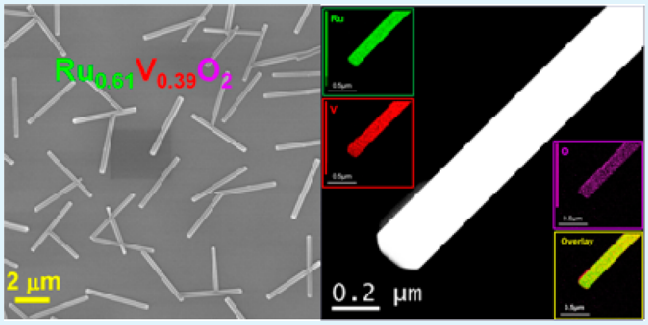

KEYWORDS: *ruthenium–vanadium mixed oxide, nanowire, electrocatalyst, H_2O_2 reduction, oxygen reduction reaction*

INTRODUCTION

Mixing two different metals with high catalytic activity to form nanostructured metal oxide materials is one area of intensive research efforts for electrocatalytic applications because of their better performance in chemical, mechanical, electrical, and optical properties compared to those of the pure metal oxides.[1−6] In particular, nanostructured mixed oxide systems composed of ruthenium dioxide (RuO_2) or iridium dioxide (IrO_2) with other metal oxides such as SnO_2, TiO_2, Ta_2O_5, VO_2, and others are some of the most fascinating materials used in the oxygen-reduction reaction (ORR), hydrogen-evolution reaction (HER), and oxygen-evolution reaction (OER) owing to their extremely high performance as electrocatalysts.[7−12] In fact, a major issue in developing mixed metal oxide catalysts is to find favorable alternatives with satisfactory activity and durability to reduce the high cost of novel metal-based electrocatalysts such as Pt, Ir, Ru, Pd, and Rh in real applications.

However, very limited processes have been previously used to obtain the thin film or nanoparticle systems for enhancing the electrochemical activity as well as stability.[13,14] Unfortunately, the mixed metal oxides used often present significant local inhomogeneity in the crystal structure, which can result in poorly defined crystal structures compared to those of single phases. Thus, it has been quite challenge to obtain well-defined single crystalline mixed metal oxides for a variety of applications.

However, very recently, we reported a facile synthesis approach for growing highly single crystalline quasi 1D $Ir_xRu_{1-x}O_2$ nanostructures via a simple vapor-phase transport process as well as their characterization by Raman scattering.[15] In our previous work, because metal oxides have the same tetragonal crystal structure and the similar ionic radius in the tetravalent ionic state, a binary mixture system of IrO_2–RuO_2 readily formed a continuous solid solution in the whole range of the composition.[15] Interestingly, well-defined 1D nanostructures in mixed forms between metal oxides are of greatly interest because of their unique advantages[16,17] compared to thin film or nanoparticle approaches. Although a binary mixture system of IrO_2–RuO_2 is remarkably attractive owing to its having the highest performance in regards to its electrocatalytic activity in the field of electrochemical catalysts, it still suffers from having a very high cost to make the single crystalline $Ir_xRu_{1-x}O_2$ nanostructures. One of the alternative strategies to

Received: May 2, 2013
Accepted: August 13, 2013
Published: August 13, 2013

 © 2013 American Chemical Society dx.doi.org/10.1021/am4016445 | ACS Appl. Mater. Interfaces 2013, 5, 8401−8406

overcome this issue is to incorporate other cheaper metals (Ta, Ti, Sn, V, Bi, etc.) into IrO_2 or RuO_2 metal oxides while retaining their fundamental electrochemical properties.

Along this research direction, the rutile RuO_2−VO_2 solid solutions have been suggested to be one of the promising candidates for electrochemical catalysts. For the binary system of $Ru_{1-x}V_xO_2$, however, only a couple of traditional synthesis methods, such as the polymerizable-complex and sol−gel methods, have been reported, which were used for making electrochemical supercapacitors.[18,19] Although $Ru_{1-x}V_xO_2$ nanoparticles showed an excellent charge-storage capacity[18,19] that is comparable to well-known pure amorphous hydrated RuO_2 nanoparticle systems, their fundamental properties in the single phase, such as their crystal structure, composition, and electrochemical behavior, were not well described because of their lack of a high quality of single crystalline $Ru_{1-x}V_xO_2$ nature. Furthermore, no one has yet reported the synthesis of high quality single crystalline $Ru_{1-x}V_xO_2$ nanowires and the study of their fundamental electrochemical behaviors for use as efficient electrocatalysts.

Therefore, in the work presented here, we have carried out the first attempts to introduce a simple process for growing single crystalline $Ru_{1-x}V_xO_2$ nanowires on a SiO_2 substrate as well as a commercial Au microwire over a broad range of Ru/V metal ratios. We have also studied their fundamental electrochemical responses, including H_2O_2-reduction and oxygen-reduction reactions (ORR).

EXPERIMENTAL SECTION

Single crystalline $Ru_{1-x}V_xO_2$ mixed oxide nanowires were directly prepared on a Si(001) wafer and on a commercial Au microwire (diameter of 25 μm) via a vapor-phase transport process using RuO_2 and VO_2 without any foreign catalyst at atmospheric pressure.[15,20] Because the vapor-phase transport process was described in detail in our recently published works,[15,20−22] only the differences in the method as it was used in the present work are given here. In this study, $Ru_{1-x}V_xO_2$ nanostructures were obtained using homogeneous mixtures by adjusting of the relative ratios of RuO_2 and VO_2 (99.9%, Aldrich) powders. The growth proceeded using helium (99.999%, 400−450 sccm) and oxygen (99.9%, 1−5 sccm) as carrier gases for 1 h. The growth substrate was placed ∼14 cm downstream from the source region, which is the temperature region of 1000 °C under the growth conditions. However, the temperature near the growth region was measured to be approximately 870 °C.

Scanning electron microscopy (SEM) and micro Raman spectroscopy were used to characterize the nanostructures obtained from our growth processes. To explore the crystal structures, an X-ray diffraction pattern was recorded with a Rigaku diffractometer using Ni filtered Cu Kα radiation, λ = 0. 15418 nm, at room temperature. In addition, high-resolution transmission electron microscopy (HRTEM, Cs-corrected STEM, JEOL JEM-2100F) at 200 kV was employed to view the images of the crystal structures for single $Ru_{1-x}V_xO_2$ mixed oxide nanowires. Topographical images were taken with an AFM (Park Systems XE-70) in an acoustic box at room temperature. The AFM tip was one of the PointProbe series from Nanosensors, Inc. (910M-NCHR), with a resonance frequency of 330 kHz and a spring constant of 42 N/m. The radius of curvature at the tip apex was nominally less than 10 nm. The AFM images were obtained using the noncontact mode at 512 × 512 pixels at a 0.2 Hz scan rate.

To investigate the electrochemical properties, the prepared $Ru_{1-x}V_xO_2$ (x = 0.28 and 0.66)-decorated Au was glued to a W wire with silver conductive paste, which was immersed vertically in an electrolyte solution up to 300 μm deep, as in our previous works.[21−23]A CHI 920C scanning electrochemical microscope (SECM, CH Instruments) was used for the electrochemical experiments where the electrode was positioned via the z axis controller of the SECM. For the auxiliary and reference electrodes, a Pt coil and saturated calomel electrode (SCE) were used, respectively.

Oxygen reduction was examined in an O_2-saturated phosphate buffer solution (0.10 M PBS, pH 7.40) using the linear sweep voltammetry (LSV) technique. The amperometric response of the $Ru_{0.34}V_{0.66}O_2$-decorated Au (or bare Au) against the concentration of H_2O_2 was monitored at E_{app} = −0.20 V (vs SCE), where the various concentrations of H_2O_2 were achieved by standard H_2O_2 addition into the PBS solution while stirring.[21,22] Most of the chemicals were purchased at Sigma-Aldrich. All other reagents and solvents were analytical grade and used as received. Deionized water (resistivity ≥18 MΩ cm) was used to prepare all aqueous solutions.

RESULTS AND DISCUSSION

Figure 1 presents typical SEM images for $Ru_{1-x}V_xO_2$ (x = 0.39) nanowires grown on a SiO_2 substrate. Interestingly, it is

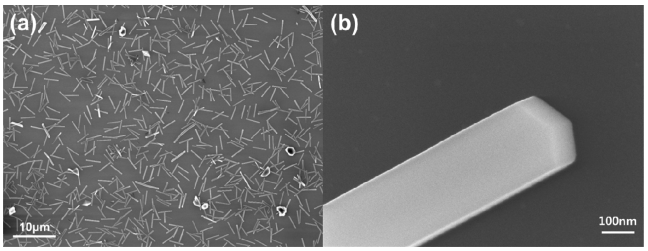

Figure 1. SEM images of as-grown $Ru_{0.61}V_{0.39}O_2$ mixed metal oxide nanowires on a SiO_2 substrate by a vapor-phase transport process.

immediately apparent that most of the nanowires were grown in the plane of the substrate, resembling the previous pure VO_2 nanowires grown[25,26] on the SiO_2 substrate. The SEM images reveal that the nanowires have the typical rectangular shape as well as sharp facets from the end of tip (Figure 1b). Furthermore, it is clear that well-defined 1D nanostructure architectures can be directly grown on the surface of an Au microelectrode for facile electrochemical applications, as shown Figure S1.[21−24] The growth of the nanowires presents a quite similar behavior, indicating an almost in-plane growth on an Au microelectrode. In particular, it should be noted that the dimensional distributions for the as-grown nanowires on a SiO_2 substrate are remarkably narrow, as shown in Figure 2. The average lateral dimension and length of the nanowires were carefully estimated by high-magnification SEM images to be 182 ± 18 nm and 3.2 ± 0.08 μm, respectively. In addition, atomic force microscopy (AFM) measurements in Figure 2c clearly confirm that the height distribution of the nanowires is extremely narrow, with an average height of ∼120 nm along the line scan profile. However, both the dimension and the dimensional distribution of $Ru_{1-x}V_xO_2$ nanowires on an Au microwire are much larger and more broad than those of a SiO_2 substrate, probably because of the difference of the surface energy in the growth mode (Figure S1).

Additionally, because the grown nanowires do not have any foreign catalytic particles at the end of the tip (Figure 1b), the well-known vapor−liquid−solid (VLS) growth mechanism is not appropriate for explaining the growth behavior of $Ru_{1-x}V_xO_2$ nanowires in our study.[21] However, it is clearly seen that there are many dropletlike structures near the nanowires (Figure S2). The droplet density is also dramatically depleted near the nanowires, implying that the dropletlike structures are being consumed into the formation of the nanowires during the period of the growth process.[25] This kind of behavior was recently observed for pure VO_2 nanowire

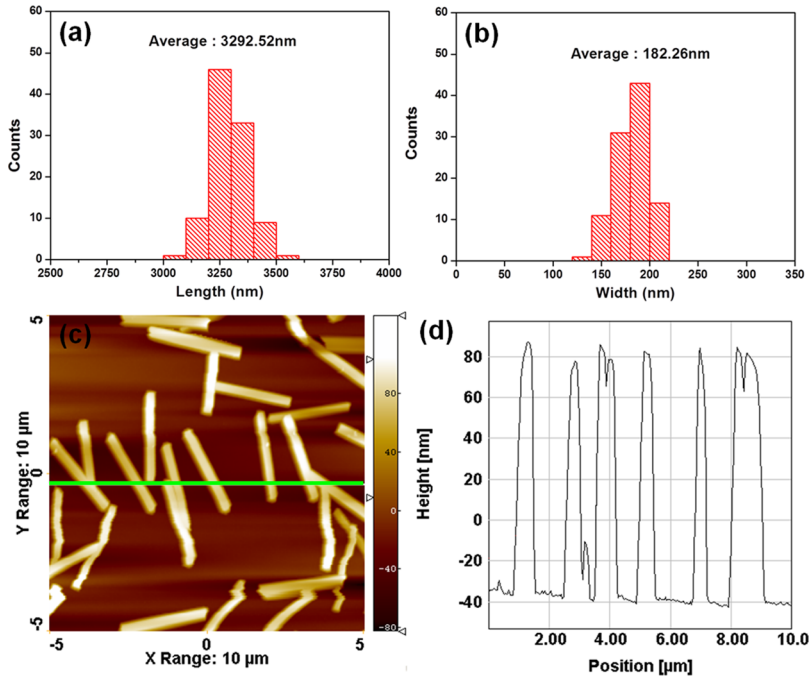

Figure 2. (a, b) Histogram of nanowire widths and lengths determined by SEM for $Ru_{0.61}V_{0.39}O_2$ mixed metal oxide nanowires grown on an SiO_2 substrate. (c) AFM image of as-grown mixed metal oxide nanowires of $Ru_{0.61}V_{0.39}O_2$ in the area of $10 \times 10\ \mu m^2$. (d) Height distribution of as-grown mixed metal oxide nanowires of $Ru_{0.61}V_{0.39}O_2$ along the line scan profile from the AFM image in panel c.

Table 1. Atomic Compositions of Various $Ru_{1-x}V_xO_2$ ($0 \le x \le 1$) Mixed Metal Oxide Nanowires Estimated by SEM-EDS Measurements[a]

source			atomic %		$Ru_{1-x}V_xO_2$		
RuO_2 (mg)	V_2O_4 (mg)	weight ratio (RuO_2/V_2O_4)	Ru	V	Ru/V	$(1-x)_{Ru}$	x_V
						1	0
14.2	1.00	14.2	16.54	2.94	5.56	0.85 (±0.02)	0.15 (±0.02)
5.70	1.00	5.70	6.10	2.47	2.44	0.71 (±0.01)	0.29 (±0.01)
5.00	0.60	8.33	3.30	2.17	1.52	0.61 (±0.01)	0.39 (±0.01)
4.40	0.90	4.89	1.91	1.45	1.32	0.57 (±0.02)	0.43 (±0.02)
2.60	2.90	0.90	3.41	3.08	1.11	0.53 (±0.02)	0.47 (±0.02)
2.00	2.00	1.00	2.10	2.46	0.85	0.46 (±0.01)	0.54 (±0.01)
4.10	1.70	2.41	4.06	6.15	0.66	0.40 (±0.01)	0.60 (±0.01)
						0	1

[a]The error bars were carefully estimated by measuring 15 different nanowires for each composition.

growth induced by supercooled liquid nanodroplets, which was carefully probed by in situ GISAXS (grazing incident small-angle X-ray scattering) measurements.[25] On the basis of careful inspection, although a more detailed mechanistic study is required, it could be proposed that the plausible growth mechanism is quite similar with that of VO_2 nanowires, so the nanodroplets might be involved in the growth process in the formation of $Ru_{1-x}V_xO_2$ nanowires.

In fact, for a binary mixture system of RuO_2–VO_2, it was reported that a continuous solid solution can be readily obtained over a broad range of compositions between the two metal oxides.[16] This is likely due to the similar ionic sizes for the Ru^{4+} (0. 0600 nm) and V^{4+} (0.0620 nm) ions, which can share the same sublattice in a tetragonal phase.[27] In our growth process, because gas-phase intermediates of RuO_4 and V_2O_5 with much lower melting points can be readily formed by oxidation from a small amount of an O_2 gas flow at such a high temperature, the growth could be explained by the preferential nucleation for VO_x and RuO_x intermediates in the gas phase.[20,25] Interestingly, the nanowire growth was highly dependent on the content of the oxygen gas at the growth temperature (Figure S3).[15,22] Without oxygen gas flow, the nanowire growth was rarely obtained. As a consequence, the morphologies of $Ru_{1-x}V_xO_2$ under high oxygen flow (20 sccm) were close to microsized crystals with sharp crystal facets (Figure S3). Thus, in our work, high aspect ratios of $Ru_{1-x}V_xO_2$ nanowires were only obtained under the limited oxygen flow rates between 1 and 5 sccm. It would be expected that these volatile species could be in the form of nanodroplets initially, which are strongly suppressed at the freezing point because of their smaller size and strongly bound nature with the substrate.[25] In the next process, two precursors in nanodroplets could be completely dissolved with each other to make a liquid solution. These mixed nanodroplets could be grown by Ostwald ripening and then supercooled before starting the crystallization on the substrate. From this process, a variety of compositions of $Ru_{1-x}V_xO_2$ mixed metal oxide nanowires can be produced.[25] According to the rigorous EDX measurements

dx.doi.org/10.1021/am4016445 | ACS Appl. Mater. Interfaces 2013, 5, 8401–8406

in Table 1, the chemical compositions of the present $Ru_{1-x}V_xO_2$ nanowires were quantitatively determined. However, it should be noted that well-defined $Ru_{1-x}V_xO_2$ mixed metal oxide nanowires with a vanadium content higher than x = 0.70 were rarely obtained in our study.

X-ray diffraction patterns prove that the $Ru_{1-x}V_xO_2$ nanowires possess a highly single crystalline nature for various compositions, as shown in Figure S4. All X-ray diffraction patterns for $Ru_{1-x}V_xO_2$ mixed metal oxide nanowires exhibit only two sharp major peaks, around 28 and 57°, with a minor satellite peak at the position near 40°, which could be attributed to the (110), (220), and (200) indexed crystallographic planes and are very consistent with the rutile structure of both pure RuO_2 and VO_2 in the tetragonal phase from the standard data (JCPDS 43-1027 for RuO_2 and 44-0253 for VO_2).[20,25] Only a few indexed peaks for $Ru_{1-x}V_xO_2$ nanowires originate from the top crystal plane of the nanowires with a rectangular cross section owing to the preferential growth in the plane of the substrate. Furthermore, Figure 3a clearly represents the

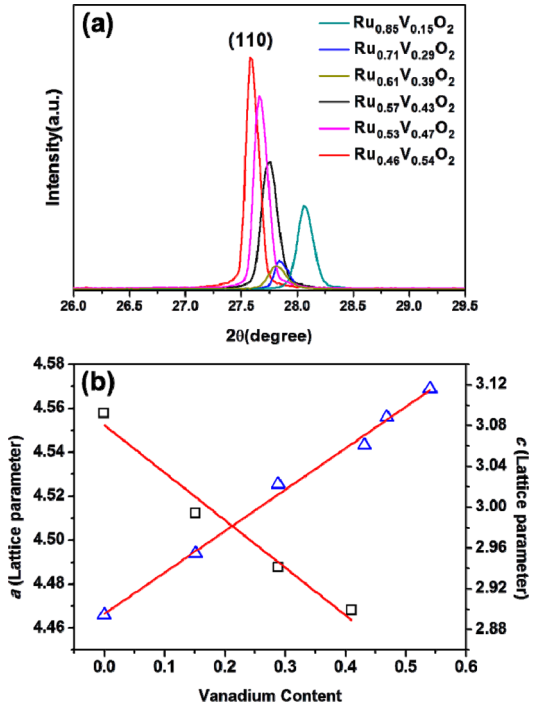

Figure 3. (a) Variation of the peak position for the (110)-indexed crystal plane of the tetragonal structure from the measured X-ray diffraction patterns as a function of the atomic ratios of two metals (Ru/V) in the mixed oxide nanowires. (b) Variation of the lattice parameters of a (triangle) and c (circle) for various $Ru_{1-x}V_xO_2$ mixed metal oxide nanowires in the tetragonal crystal structure as a function of the vanadium (V) content. Note that the units of the lattice parameters of a and c are in angstroms (Å).

continuous variation of the peak position for a (110)-indexed crystal plane with respect to the relative contents of two metals in the mixed oxide nanowires, indicating the homogeneous formation of the continuous solid solution from both pure RuO_2 and VO_2 crystal structures. We have quantitatively estimated the lattice parameters from our XRD data using Bragg's equation as a function of the V atom content. Although the lattice constants of a were easily calculated from XRD data, the lattice constant of c could not be extracted from our measured XRD data because of the absence of the c axis-containing crystallographic plane resulting from the highly oriented growth behavior of the $Ru_{1-x}V_xO_2$ nanowires in the plane on a SiO_2 substrate. Therefore, to obtain the lattice constant of c, we had to mechanically grind the $Ru_{1-x}V_xO_2$ nanowires on a SiO_2 substrate to break them from the substrate. As a consequence, the XRD patterns after this process showed an additional indexed peak with a relatively weak intensity corresponding to (011) or (101), as shown in Figure S5. Thus, Figure 3b indicates that the lattice parameters of $Ru_{1-x}V_xO_2$ nanowires vary linearly with the vanadium content for a continuous substitutional solid solution, closely following the prediction of Vegard's rule[28] for an ideal solid solution.

Figure 4a,b represents typical HRTEM images of a single $Ru_{0.59}V_{0.41}O_2$ nanowire along the zone axis of [1-10], indicating

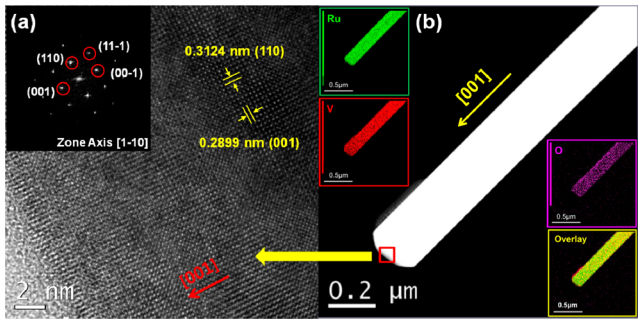

Figure 4. (a) Lattice resolved HRTEM image of a single $Ru_{0.59}V_{0.41}O_2$ mixed metal oxide nanowire. The inset shows the fast Fourier transform (FFT) of the lattice-resolved image. (b) High-angle annular dark field (HAADF) STEM image and EDS-elemental mapping analysis for Ru(L) and V(M) atoms of a single $Ru_{0.59}V_{0.41}O_2$ mixed metal oxide nanowire.

that the nanowire is single crystalline in nature. In addition, there is no evidence for alternative structures such as $(VO_2)_x/(RuO_2)_{1-x}$ core/shell or layered structures. The distances of the adjacent crystal planes are estimated to be about 0.3124 and 0.2899 nm from the lattice-resolved HRTEM image, corresponding to the (110) and (001) crystallographic interplanar distances of the tetragonal RuO_2 and VO_2 unit cells, respectively. Consequently, our results clearly indicate that the spacing of the (110) and (001) planes are slightly shifted along the incorporation of the relative amounts of two metal ions into the tetragonal lattice from two pure metal oxides, consistent with the results of the X-ray diffraction patterns. In addition, the mixed oxide nanowire grows along the [001] direction from the fast Fourier transform (FFT) of the lattice-resolved image in Figure 4a (inset). Furthermore, the spatial distributions of all elements on a single $Ru_{1-x}V_xO_2$ mixed oxide nanowire shown in a high-angle annular dark field (HAADF) STEM image represent a highly homogeneous distribution in the whole part of the nanowire in Figure 4b. This observation also supports the formation of a homogeneous solid solution of an RuO_2–VO_2 mixed metal oxide system.

To investigate the electrochemical behavior of the prepared $Ru_{1-x}V_xO_2$ raised on a single piece of Au microwire ($Ru_{1-x}V_xO_2$–Au microelectrode), CV voltammograms of $Ru_{1-x}V_xO_2$–Au microelectrodes were obtained by immersing them 300 μm-deep in an aqueous electrolyte solution (1.0 M KCl) containing cationic or anionic electroactive species $(Ru(NH_3)_6^{3+}$ or $[Fe(CN)_6]^{3-})$. The CV pattern of the

dx.doi.org/10.1021/am4016445 | ACS Appl. Mater. Interfaces 2013, 5, 8401–8406

$Ru_{0.34}V_{0.66}O_2$–Au in a 10 mM $[Fe(CN)_6]^{3-}$ solution shows a gradual change from a peak-shaped wave to a steady-state one as the potential scan rate (ν) decreases because of the time-dependent growth pattern of the diffusion layer, as discussed in our previous works[21−23] (Figure 5a). In Figure 5b quasi-steady-

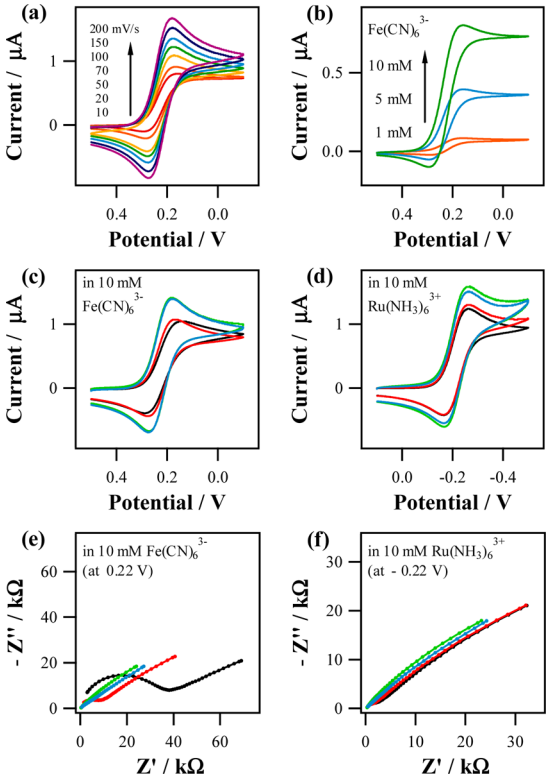

Figure 5. (a) CV plots of $Ru_{0.34}V_{0.66}O_2$–Au in a 1.0 M KCl solution containing 10 mM $Fe(CN)_6^{3-}$ at different scan rates (10, 20, 50, 70, 100, 150, and 200 mV s^{-1}). (b) CV plots of $Ru_{0.34}V_{0.66}O_2$–Au in a 1.0 M KCl solution with three different concentrations of $Fe(CN)_6^{3-}$ (1, 5, and 10 mM) at a scan rate (ν) of 10 mV s^{-1}. (c, d) CV plots in a 1.0 M KCl solution containing (c) 10 mM $Fe(CN)_6^{3-}$ and (d) 10 mM $Ru(NH_3)_6^{3+}$ with ν of 100 mV s^{-1}. (e, f) Nyquist plots of electrodes at (e) 0.22 V and (f) −0.22 V in the frequency range from 1 Hz to 10 kHz. The other conditions in panel e are the same as those in panel c, whereas those in panel f, as in panel d. Bare Au wire (d = 25 μm) (black), bare Pt wire (d = 25 μm) (red), $Ru_{0.34}V_{0.66}O_2$–Au (green), and $Ru_{0.72}V_{0.28}O_2$–Au (blue).

state current values at −0.1 V (with ν of 10 mV s^{-1}) shows a linear relationship with the concentration of $[Fe(CN)_6]^{3-}$ (1, 5, and 10 mM) using $Ru_{0.34}V_{0.66}O_2$–Au. The general electrochemical activity of the prepared $Ru_{1-x}V_xO_2$–Au that was dependent on the composition was compared with the CV waves of bare microwire electrodes (Au or Pt, diameter = 25 μm) at ν of 0.1 V s^{-1}. The CV curves of $Ru_{0.72}V_{0.28}O_2$–Au and $Ru_{0.34}V_{0.66}O_2$–Au show decent electrochemical behaviors compared to that of the bare Pt or Au electrode for both negatively and positively charged redox couples (i.e., $[Fe(CN)_6]^{3-/4-}$ and $Ru(NH_3)_6^{3+/2+}$) (Figure 5c,d), supporting favorable electrode kinetics and implying that $Ru_{0.34}V_{0.66}O_2$, up to about 70% of metal exchange from RuO_2, still shows good electrical conductivity as an electrode material. This metallic property of $Ru_{1-x}V_xO_2$ along with the electron microscopy data also supports the idea that VO_2 has a rutile-type structure.[18] To confirm the electron-transfer kinetics of the $Ru(NH_3)_6^{3+/2+}$ and $[Fe(CN)_6]^{3-/4-}$ couple at the electrode surface, electrochemical impedance spectroscopy (EIS) experiments were carried out under the same condition as those used in the CV experiments. Nyquist plots of $Ru_{1-x}V_xO_2$–Au (x = 0.28 and 0.66) in both $[Fe(CN)_6]^{3-}$ and $Ru(NH_3)_6^{3+}$ solutions within the frequency range from 1 Hz to 10 kHz reveal straight lines, which implies Nernstian reversibility, similar to that of bare Pt (Figure 5e,f). Meanwhile, bare Au showed a semicircle at higher frequencies, especially in the $[Fe(CN)_6]^{3-}$ solution, which is unlike $Ru_{1-x}V_xO_2$–Au or bare and is probably due to the relatively high charge-transfer resistance. The EIS result also supports the high electroactivity of $Ru_{1-x}V_xO_2$–Au (x = 0.28 and 0.66) for the ferri/ferrocyanide redox couple.

The electrocatalytic activity of $Ru_{1-x}V_xO_2$–Au (x = 0.28 and 0.66) toward the oxygen-reduction reaction (ORR) was investigated in an O_2-saturated 0.10 M PBS (pH 7.40) solution using the LSV technique. As shown in Figure 6a, $Ru_{0.34}V_{0.66}O_2$

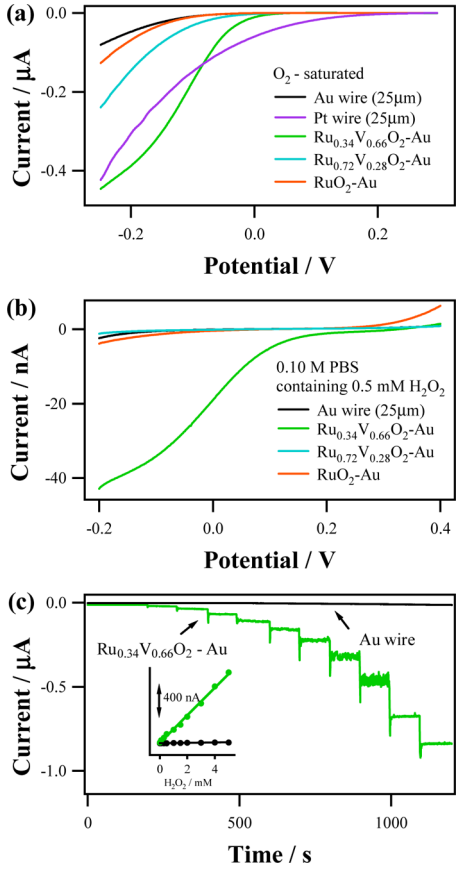

Figure 6. (a) Background-corrected LSV measurements for the ORR in an O_2-saturated 0.10 M phosphate buffer solution (PBS, pH 7.40) with ν of 10 mV s^{-1}. (b) Background-corrected LSV measurements in 0.10 M PBS containing 0.5 mM H_2O_2 with ν of 10 mV s^{-1}. (c) Dynamic current responses of the bare Au micowire and $Ru_{0.34}V_{0.66}O_2$–Au to the increases in the H_2O_2 concentration in 0.10 M PBS at E_{app} = −0.2 V vs SCE (inset: corresponding calibration plots).

–Au revealed higher ORR activity than any other electrode except Pt, which could be applicable to a biofuel cell cathode. Because $Ru_{0.34}V_{0.66}O_2$–Au showed decent ORR activity, we examined further its electrochemical sensing of H_2O_2, which is applicable to the broad field of enzyme-based biosensors. In the LSV measurement (Figure 6b), a negligible H_2O_2 redox reaction was observed for bare Au and $Ru_{0.72}V_{0.28}O_2$–Au, but

dx.doi.org/10.1021/am4016445 | ACS Appl. Mater. Interfaces 2013, 5, 8401−8406

a significant cathodic current of H_2O_2 reduction was observed for $Ru_{0.34}V_{0.66}O_2$–Au, which was different from the significant H_2O_2 oxidation for a RuO_2 nanorod.[23] Figure 6c presents the typical amperometric response curves (i–t curves) of the $Ru_{0.34}V_{0.66}O_2$–Au electrode in response to consecutive increments of H_2O_2 at −0.20 V in deoxygenated 0.10 M PBS (pH 7.40). The amperometric response is fast enough (<1.0 s) and increases linearly, depending on the concentration of H_2O_2, with a proportional slope (sensitivity) of 160 nA mM^{-1} (r = 0.998) and a detection limit of 22 μM. This clearly suggests that H_2O_2 reduction is remarkably facilitated by $Ru_{0.34}V_{0.66}O_2$–Au. The other positive characteristics of the $Ru_{0.34}V_{0.66}O_2$–Au electrode are the selectivity against biological interferents and the operational stability, as shown in Figure S6 of the Supporting Information.

CONCLUSIONS

We report the novel process for preparing single crystalline $Ru_{1-x}V_xO_2$ nanowires in a broad range of compositions by a simple vapor-phase transport process with pure RuO_2 and VO_2. Upon extensive microscopic observations, single crystalline $Ru_{1-x}V_xO_2$ mixed metal oxide nanowires show well-defined homogeneous solid-solution characteristics as well as the distinct feature of having a remarkably narrow dimensional distribution. All of the electrochemical observations regarding $Ru_{1-x}V_xO_2$–Au (x = 0.28, 0.66) indicate the favorable charge-transfer kinetics of $[Fe(CN)_6]^{3-/4-}$ and $[Ru(NH_3)_6]^{3+/2+}$ at the $Ru_{1-x}V_xO_2$ surface, where the metallic properties of $Ru_{1-x}V_xO_2$ were also confirmed. $Ru_{0.34}V_{0.66}O_2$–Au revealed a high ORR activity and a selective amperometric response toward H_2O_2. Overall, we have characterized the electrochemical properties of new material, $Ru_{1-x}V_xO_2$–Au (x = 0.28, 0.66), and we have demonstrated clearly that a $Ru_{0.34}V_{0.66}O_2$–Au microelectrode has features that are attractive for use as a biofuel cell cathode or amperometric H_2O_2 sensor. Finally, our continuing efforts to manufacture metal oxide-decorated microelectrodes and their characterization have provided unique multiscale architectures with highly crystalline 1D nanostructures. The present work is the first report for RuO_2–VO_2 mixed metal oxide nanowires and furthermore it can be easily extended toward other promising systems.

ASSOCIATED CONTENT

Supporting Information

SEM images of various compositions for $Ru_{1-x}V_xO_2$ mixed metal oxide nanowires grown on a 25 μm Au microwire, SEM images and a EDX line scan of various compositions for $Ru_{1-x}V_xO_2$ mixed metal oxide nanowires on a SiO_2 substrate, SEM images for as grown $Ru_{1-x}V_xO_2$ under gas flows with 0 and 20 sccm of O_2, X-ray diffraction patterns of $Ru_{1-x}V_xO_2$ nanowires, X-ray diffraction patterns for ground samples for various $Ru_{1-x}V_xO_2$ mixed metal oxide nanowires on a SiO_2 substrate, and dynamic current responses of $Ru_{0.34}V_{0.66}O_2$–Au. This material is available free of charge via the Internet at http://pubs.acs.org.

AUTHOR INFORMATION

Corresponding Authors

*E-mail: cmlee@ewha.ac.kr (C.L.).
*E-mail: myungkim@ewha.ac.kr (M.H.K.).

Author Contributions

‖These authors contributed equally to this work.

Notes

The authors declare no competing financial interest.

ACKNOWLEDGMENTS

This research was supported by MEST (Ministry of Education, Science and Technology) & DGIST (13-BD-01, Convergence Technology with New Renewable Energy and Intelligent Robot) and by the Basic Science Program through the National Research Foundation of Korea (NRF) funded by MEST (nos. 2013-020688 and 2010-0022028).

REFERENCES

(1) Banger, K. K.; Yamashita, Y.; Mori, K.; Peterson, R. L.; Leedham, T.; Rickard, J.; Sirringhaus, H. *Nat. Mater.* **2011**, *10*, 45.
(2) Sun, J. M.; Zhu, K. K.; Gao, F.; Wang, C. M.; Liu, J.; Peden, C. H. F.; Wang, Y. *J. Am. Chem. Soc.* **2011**, *133*, 11096.
(3) Trotochaud, L.; Boettcher, S. W. *Chem. Mater.* **2011**, *23*, 4920.
(4) Trasatti, S. *Electrochim. Acta* **2000**, *45*, 2377.
(5) Mai, L. Q.; Xu, L.; Gao, Q. A.; Han, C. H.; Hu, B.; Pi, Y. Q. *Nano Lett.* **2010**, *10*, 2604.
(6) Mai, L. Q.; Xu, X.; Han, C. H.; Luo, Y. Z.; Xu, L.; Wu, Y. M. A.; Zhao, Y. L. *Nano Lett.* **2011**, *11*, 4992.
(7) Zhao, Y. L.; Xu, L.; Mai, L. Q.; Han, C. H.; An, Q. Y.; Xu, X.; Liu, X.; Zhang, Q. J. *Proc. Natl. Acad. Sci. U.S.A.* **2012**, *109*, 19569.
(8) Sardar, K.; Ball, S. C.; Sharman, J. D. B.; Thompsett, D.; Fisher, J. M.; Smith, R. A. P.; Biswas, P. K.; Lees, M. R.; Kashtiban, R. J.; Sloan, J.; Walton, R. I. *Chem. Mater.* **2012**, *24*, 4192.
(9) Allam, N. K.; Alamgir, F.; El-Sayed, M. A. *ACS Nano* **2010**, *4*, 5819.
(10) Lyons, M. E. G.; Floquet, S. *Phys. Chem. Chem. Phys.* **2011**, *13*, 5314.
(11) Li, G.; Yu, H.; Wang, X.; Sun, S.; Li, Y.; Shao, Z.; Yi, B. *Phys. Chem. Chem. Phys.* **2013**, *15*, 2858.
(12) Owe, L. E.; Tsypkin, M.; Wallwork, K. S.; Haverkamp, R. G.; Sunde, S. *Electrochim. Acta* **2012**, *70*, 158.
(13) Mattos-Costa, F. I.; de Lima-Neto, P.; Machado, S. A. S.; Avaca, L. A. *Electrochim. Acta* **1998**, *44*, 1515.
(14) Cheng, J.; Zhang, H.; Ma, H.; Zhong, H.; Zou, Y. *Electrochim. Acta* **2010**, *55*, 1855.
(15) Lee, Y.; Shin, H. Y.; Chun, S. H.; Lee, J.; Park, W. J.; Baik, J. M.; Yoon, S.; Kim, M. H. *J. Phys. Chem. C* **2012**, *116*, 16300.
(16) Yang, X. Y.; Wolcott, A.; Wang, G. M.; Sobo, A.; Fitzmorris, R. C.; Qian, F.; Zhang, J. Z.; Li, Y. *Nano Lett.* **2009**, *9*, 2331.
(17) Szot, K.; Speier, W.; Bihlmayer, G.; Waser, R. *Nat. Mater.* **2006**, *5*, 312.
(18) Yokoshima, K.; Shibutani, T.; Hirota, M.; Sugimoto, W.; Murakami, Y.; Takasu, Y. *J. Power Sources* **2006**, *160*, 1480.
(19) Yuan, C. Z.; Gao, Y. B.; Zhang, X. G. *J. Power Sources* **2007**, *173*, 606.
(20) Lee, Y.; Ye, B.-U.; Yu, H. K.; Lee, J.-L.; Kim, M. H.; Baik, J. M. *J. Phys. Chem. C* **2011**, *115*, 4611.
(21) Shim, J. H.; Lee, Y.; Kang, M.; Lee, J.; Baik, J. M.; Lee, Y.; Lee, C.; Kim, M. H. *Anal. Chem.* **2012**, *84*, 3827.
(22) Lee, Y.; Kang, M.; Shim, J. H.; Lee, N.-S.; Baik, J. M.; Lee, Y.; Lee, C.; Kim, M. H. *J. Phys. Chem. C* **2012**, *116*, 18550.
(23) Kang, M.; Lee, Y.; Jung, H.; Shim, J. H.; Lee, N.-S.; Baik, J. M.; Lee, S. C.; Lee, C.; Lee, Y.; Kim, M. H. *Anal. Chem.* **2012**, *84*, 9485.
(24) Shim, J. H.; Kang, M.; Lee, Y.; Lee, C. *Microchim. Acta* **2012**, *177*, 211.
(25) Kim, M. H.; Lee, B.; Lee, S.; Larson, C.; Baik, J. M.; Yavuz, C. T.; Seifert, S.; Vadja, S.; Winans, R. E.; Moskovits, M.; Stucky, G. D.; Wodtke, A. M. *Nano Lett.* **2009**, *9*, 4138.
(26) Baik, J. M.; Kim, M. H.; Larson, C.; Wodtke, A. M.; Moskovits, M. *J. Phys. Chem. C* **2008**, *112*, 13328.
(27) Takasu, Y.; Nakamura, T.; Ohkawauchi, H.; Murakami, Y. *J. Electrochem. Soc.* **1997**, *144*, 2601.
(28) Wang, X.; Hanson, J. C.; Rodriguez, J. A.; Belver, C.; Fernandez-Garcia, M. *J. Chem. Phys.* **2005**, *122*, 154711.